SINDy analysis of disturbance and plant model superposition on a rolling delta wing

Conference Paper · June 2018

DOI: 10.2514/6.2018-3068

3 authors:

Mathieu Le Provost
University of California, Los Angeles
9 PUBLICATIONS **9** CITATIONS
SEE PROFILE

David Williams
Illinois Institute of Technology
112 PUBLICATIONS **1,719** CITATIONS
SEE PROFILE

Steven L. Brunton
University of Washington Seattle
206 PUBLICATIONS **4,154** CITATIONS
SEE PROFILE

SINDy analysis of disturbance and plant model superposition on a rolling delta wing

Mathieu Le Provost*
University of California, Los Angeles, Los Angeles, CA, 90095

David R. Williams†
Illinois Institute of Technology, Chicago, IL, 60616

Steven L. Brunton‡
University of Washington, Seattle, WA, 98195

Classical closed-loop controllers used in active flow control theory assume the validity of the principle of superposition to estimate the state variable response to actuation and disturbances. In this paper, we look examine the validity of the principle of superposition, which implicitly assumes the linearity of the system to control. A coupled model for the disturbance response is designed with an extended version of the Goman-Khrabrov model and a separate linear model based on sparse surface pressure measurements on the upper surface of the wing. A nonlinear model for the roll moment response of the wing to pneumatic actuation is designed with the SINDy method introduced by Brunton, et al.[1] An optimal operator to account for coupling effects between the disturbance model and actuation model is investigated using the SINDy algorithm.

Nomenclature

b	Wing span, mm
c	Chord, mm
C_l	Roll moment coefficient
C_p	Pressure coefficient $C_p = \frac{p-p_\infty}{\frac{1}{2}\rho U_\infty^2}$
f	Roll frequency, Hz
I_{xx}	Moment of inertia about X-axis, $kg.m^2$
k	Reduced roll frequency $k = \frac{\pi f c}{U_\infty}$
p_∞	Static pressure, Pa
U_∞	Free-stream velocity,m/s
U_k	Input variable at the time step k
X_k	State variable at the time step k
x_0	Nonlinear forcing term in Goman-Khrabrov equation
$\hat{X}^-$	A priori state estimate
$\hat{X}^+$	A posteriori state estimate
α	Angle of attack, $^\circ$
$\dot{\alpha}$	Pitch rate, $^\circ/s$
ϕ	Roll angle, $^\circ$
$\dot{\phi}$	Roll rate, $^\circ/s$
$\ddot{\phi}$	Roll acceleration, $^\circ/s^2$
ρ	Air density, kg/m^3
$..^+$	Moore-Penrose pseudo-inverse
,	To separate matrices in the same line
;	To separate matrices in the same column

*Graduate Research Assistant, MAE Department, 48-121 E4, AIAA Student member
†Professor, MMAE Department, 10 W. 32nd St. REC Bldg., AIAA Associate Fellow
‡Assistant Professor, Mechanical Engineering Department, MEB 305, AIAA member

I. Introduction

A common approach when designing closed-loop active flow control systems is to assume that the system response to actuation is independent of its response to external disturbances. For example, when synthetic jet actuators were used by Williams, et al.[2] to reduce the lift hysteresis that occurred on a pitching wing, separate models were identified for the lift response to the pitching motion and the lift response to the synthetic jet actuation. This is sensible, because the lift response to the global pitching wing disturbance will be completely different from the unsteady lift produced by a localized actuator input. The assumption is then made that the net lift output will be the linear superposition of these two models. Effective closed-loop controllers based on this assumption have been designed and demonstrated for numerous flow control applications Kerstens, et al.[3] However, the superposition assumes that there are no significant interactions between the external disturbance and the actuated flow. If interactions do occur, then we expect nonlinear interactions involving cross-terms of these two models.

In this paper we explore the possibility of identifying nonlinear interactions between the disturbance roll moment produced by a rolling, three-dimensional wing and the roll moments produced with trailing-edge jet actuators. Models for both are identified from experimental measurements. The system roll moments for three cases are compared: roll only, actuation only, and roll plus actuation. Differences in the roll moment between the roll plus actuation case from the sum of the roll only and actuation only cases are attributed to nonlinear effects and experimental noise. A new method known as the Sparse Identification of Nonlinear Dynamics (SINDy) introduced by Brunton, et al.[1] is used to identify the nonlinear interactions. The system model is then modified to include the strongest nonlinear terms, and its performance is assessed with experimental data.

Details of the experimental setup are provided in the next section §II. The superposition of the disturbance and actuator models, and details of the SINDy method are provided in section §III. Results from the experimental measurements of the disturbance and actuator models are presented in §IV. Design of an optimal operator using the SINDy method is discussed in §V, and the conclusions are discussed in §VI.

II. Experimental Setup

Data for the identification of models was obtained from experiments conducted in the Fejer Unsteady Flow Wind Tunnel at Illinois Institute of Technology. The wind tunnel test section dimensions are $600mm$ by $600mm$ in cross-section and the length of the test section is $3m$.

The wing model was a hybrid UCAS design consisting of a Lockheed Martin ICE-101 planform and airfoil sections taken from the NATO-AVT-Saccon design. The centerline chord was $c = 330mm$, and the span was $b = 287mm$. The planform area $S = 0.0474m^2$. The moment of inertia about the X-axis, $I_{xx} = 3.12x10^{-4}kg.m^2$, where the positive X-axis is aligned with the root chord of the wing pointing forward from the apex of the model. The flow speed was $6.5m/s$ and the Reynolds number based on the chord was 142,000. The wing was instrumented with 12 surface pressure sensors (Allsensors 5 inch H20). The sensors were mounted internally with 1mm long ports connecting to the wing surface. A 2D drawing of the pressure sensors position on the upper surface of the UCAS model is presented in Fig.1. A CAD drawing of the upper and lower half parts of the model is shown in Fig.2. The overall mass of the model including pressure sensors and wiring was $130g$.

Direct force and moment measurements were obtained with an ATI NANO-25 6-component balance mounted in the interior of the wing. The balance was connected directly to the sting mechanism. The center of the balance was located at the $\frac{1}{4}$ mean aerodynamic chord(mac).

The sting supporting the model allowed roll, pitch, and plunge maneuvers. The angle of attack and height of the model in the test section were controlled by two Copley servo tubes. The roll motion was driven by a high-torque R/C-servo, which was controlled by a dSPACE MicroLabBox system. The roll mechanism was equipped with a roll tube that produced roll angles between $+/-30^\circ$ with roll rates up to $3Hz$, which is equivalent to a dimensionless frequency $k = \frac{\pi fc}{U_\infty} = 0.478$.

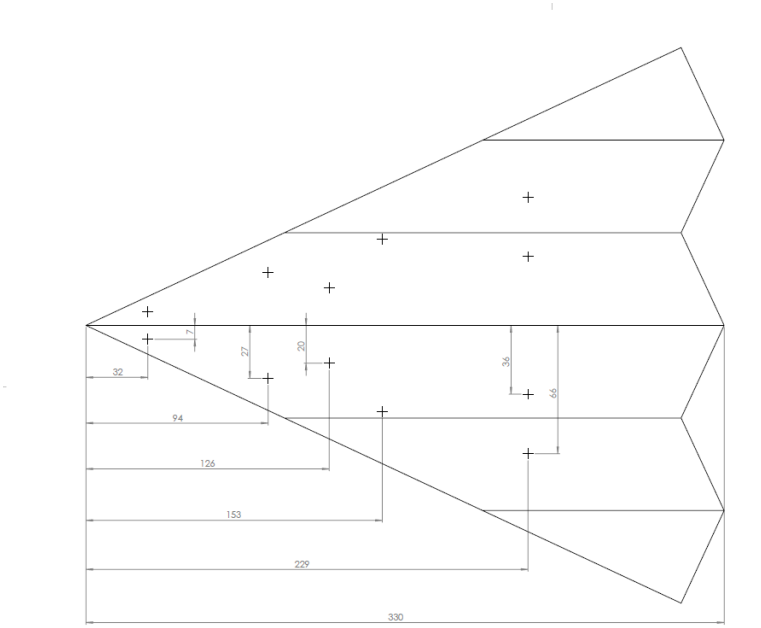

Figure 1: Plan view drawing of the pressure sensors position on the upper surface of the UCAS model (scale is in mm)

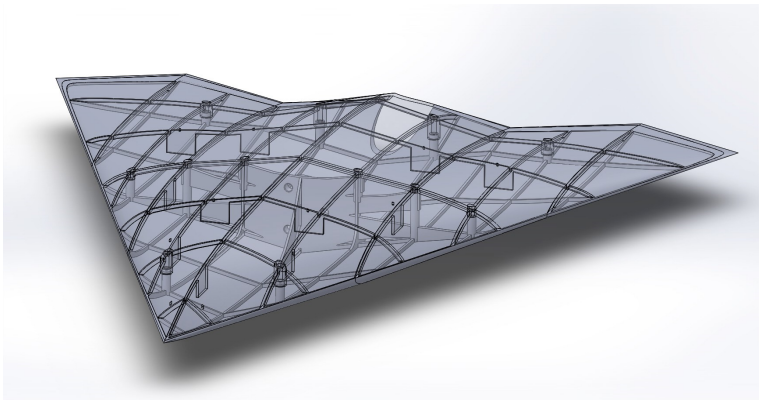

Figure 2: CAD drawing of UCAS model upper and lower halves

The roll control actuators consist of a pair of downward-blowing pneumatic actuators at the left(port) and right (starboard) trailing edges of the wing Fig.3. The actuator slot dimensions are $30mm$ length and a slot opening width of $0.2mm$. The exiting flow blows downward at an approximate angle of 90° to the chordline of the wing. The flow rate through each actuator is given in a non-dimensional form as the momentum coefficient C_μ, defined as $C_\mu = \frac{\dot{m} \times U_{act}}{\frac{1}{2}\rho U_\infty^2 S_{wing}}$ where $\dot{m}$ is the mass flow rate of the actuation, U_{act} is the mean speed of the actuation, ρ is the density of the air and S_{wing} is the surface of the wing. For the experiments presented in this paper we have $C_\mu < 0.009$.

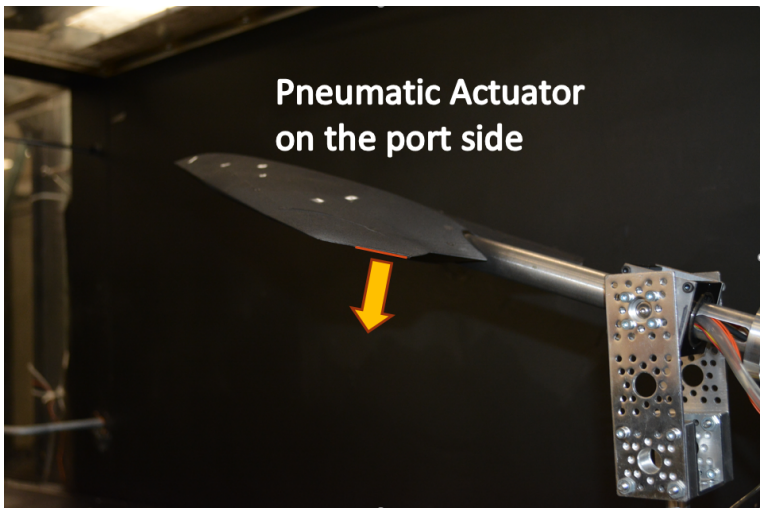

Figure 3: Pneumatic effector on the left hand side of the delta wing

III. Discussion of validity of superposition and brief description of SINDy

The design of the closed-loop controller is based on the classical control architecture introduced by King et al.[3] and used by Williams et al.[2] to control the pitch motion of an airfoil. The block diagram is shown in Fig.4. In our case, the disturbance is a roll angle ϕ, and the objective of the controller is to compensate for the disturbance roll moment.

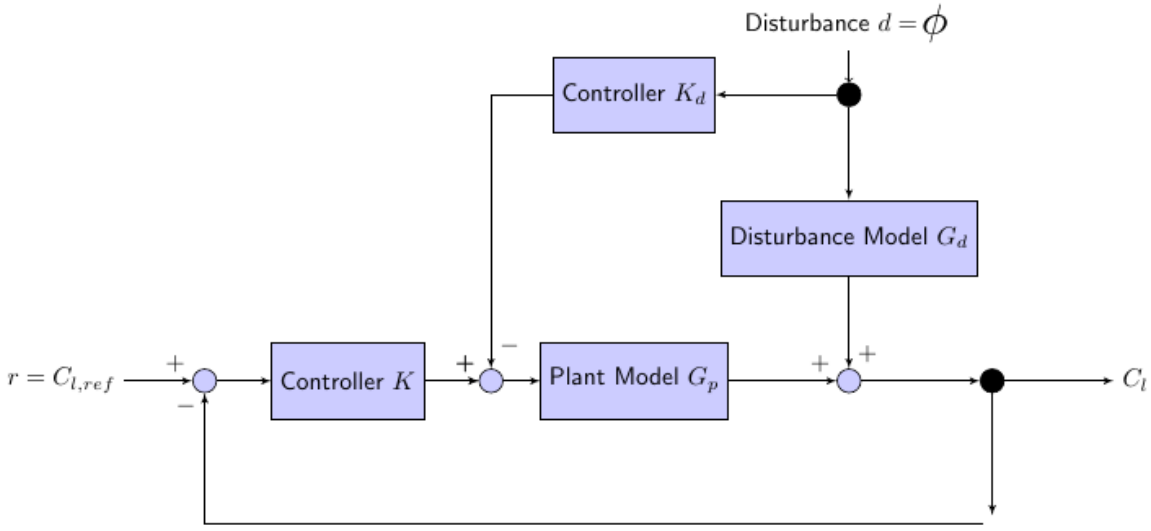

Figure 4: Control Architecture for roll moment control

The control system is composed of:

- A disturbance model G_d, i.e. the response of the system to a roll disturbance ϕ.
- A plant model G_p i.e. the response of the system subject to actuation.
- With the G_p and G_d models, we can design the feedforward K_d and feedback K controllers. The feedforward controller will be designed using the transfer function of the disturbance model, the inverted plant model and a filter for causality. The feedback controller has also to be designed.

The classical approach in the design of closed-loop controllers is to develop a model for the response to actuation and disturbances independently. Then, in the final closed-loop architecture, we get the response of the system by linearly adding the contributions of disturbance model and the actuation model. The underlying assumption is that our global system behaves linearly. In other words, we get the global response by just considering the response of the system to each contribution considered independently. The objective of this paper is to test the validity of this principle of superposition in the context of active flow control. Based on the results for the validity of this principle for the active flow control of a rolling delta wing, we will look for the design of an nonlinear optimal operator, which will be able to take into account the coupling effects between the contributions of the disturbance and actuation models.

The design of this optimal operator will be done using a new method introduced by Brunton et al.[1] for the identification of nonlinear dynamics. This method is called Sparse Identification of Nonlinear Dynamics, and it attempts to identify the governing equations from a dataset using sparsity-promoting and machine learning techniques.

The SINDy approach has been designed to overcome the problem of non-sparsity of the least-squares regression where most of the terms are active. With a sparse regression, we will be able to identify only the relevant terms in the dynamics. The SINDy algorithm combines the simplicity of the least-square regression and the interpretability and robustness of sparse models. Indeed sparse models promotes robustness, because only the relevant terms are used in the model. This algorithm is particularly interesting when we are faced with new problems, where it is difficult to guess which terms should be included to model the behavior of the system.

Let consider a dynamical system of the form:

$$\frac{dx}{dt} = f(x(t)) \tag{1}$$

The vector $x(t) \in \mathcal{R}^n$ denotes the state of a system at time t, and the function $f(x(t))$ represents the dynamic of the system.

The first step is to organize the time-series data using the "snapshots method". Then, we have to compute or approximate numerically the derivative $\dot{X}$ of the time-series data X. The third step is to construct a library $\theta(X)$ consisting of a large spectrum of nonlinear candidate functions of X (and inputs if there are any). For instance, $\theta(X)$ may consist of constant, polynomial and trigonometric terms:

$$\theta(X) = \begin{bmatrix} \dots & 1 & \dots \\ \dots & X & \dots \\ \dots & X^2 & \dots \\ \dots & X^p & \dots \\ \dots & cos(X) & \dots \end{bmatrix} \tag{2}$$

There are an infinite number of nonlinear candidates, but we believe that only a few of these terms are active in each line of f, we may set up a sparse regression problem to determine the sparse vector of coefficients $\Xi = \begin{bmatrix} \xi_1 & \xi_2 & \dots & \xi_n \end{bmatrix}^T$.

The sparse regression problem to solve is:

$$\dot{X} = \Xi\theta(X) \tag{3}$$

The algorithm used for sparse regression in this paper is called the sequentially thresholded least squares (STLS) that was introduced by Mezic, et al.[4] In this algorithm, we start with a least-squares solution for Ξ, and then remove all coefficients Ξ_j that are smaller than a fixed parameter λ called the cutoff value. Then

we do a new least square regression on the remaining non-zero coefficients. These new coefficients are again thresholded using λ, and the procedure is continued until the non-zero coefficients converge. This algorithm is computationally efficient, and it rapidly converges to a sparse solution in a small number of iterations. The algorithm also benefits from simplicity, with only a single parameter λ required to determine the degree of sparsity in Ξ. STLS turns out to be very effective as shown by Brunton, et al.[1]

Algorithm 1 Algorithm for STLS(θ,$\dot{X}$,λ,*tol*,iters), Brunton, et al.[1]

$\hat{\Xi}$=argmin$_\Xi$$||\dot{(X)} - \Xi\Theta(X)||_2^2$ # least square estimation
bigcoeffs=$\{$j such that $\Xi_j > \lambda\}$ # select large coefficients
$\hat{\Xi}$[smallcoeffs]=0 # remove small coefficients
$\hat{\Xi}$[bigcoeffs]=STLS(θ,$\dot{X}$,λ,iters) # Iterative procedure

III.A. Design of the disturbance model

This section is a summary of the disturbance model designed by Le Provost, et al.[5] for the roll moment response of a rolling delta wing to roll disturbance ϕ. We first designed an extended version of the Goman-Khrabrov model(eGK)[5].[6] The original Goman-Khrabrov model[6] was based on the idea that we can link the lift coefficient of an airfoil during dynamic motions to the degree of flow attachement over an airfoil. For that, they assumed that dynamic motions only create a time-delay in the degree of flow attachement compared to steady cases.

To improve the robustness of the final prediction, we also derived a model for the roll moment based on the pressure measurements on the upper surface of the wing. We first derived a time-shifted linear model introduced by Bingni Brunton et al.[7] for the pressure coefficients corrected with a Kalman filter based on the pressure measurements. We can linearly map these corrected predictions for the pressure coefficients to a prediction for the roll moment. The final prediction for the roll moment response to disturbances is obtained by combining the extended Goman-Khrabrov model (eGK) with the linear model based on pressure using again a Kalman filter. The different steps are presented in the Fig.5:

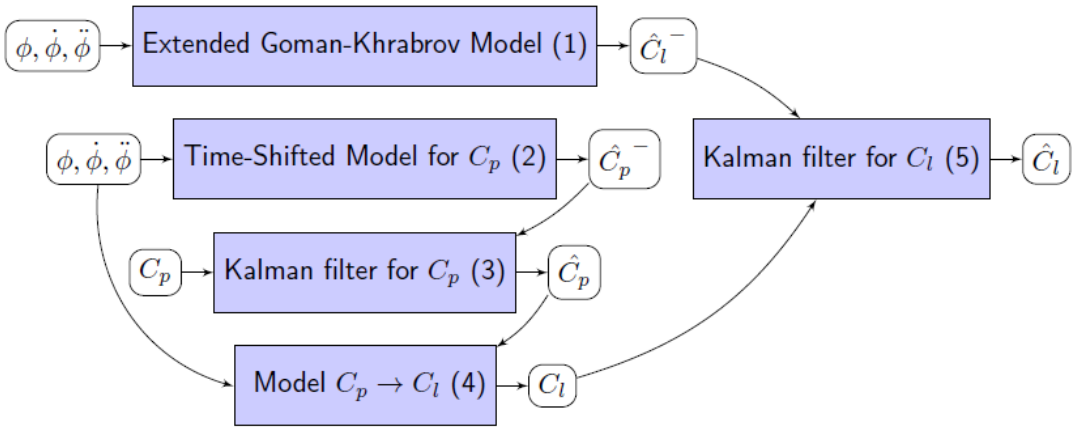

Figure 5: Coupling of the different components of the disturbance model.

III.B. Design of the actuation model

The actuation model is derived with the SINDy algorithm. The actuation input used is a random input with holds as shown in Fig.6 introduced by Brunton, et al.,[8] because holds in the inputs allow to capture quasi-steady aerodynamic effects. The pool of nonlinear candidates is composed of all the possible combination of

the variables up to the second degree i.e.:

$$\Theta(C_{l,Act,k}, C_{\mu,k}, \dot{C_{\mu,k}}, \alpha_k) = \begin{bmatrix} 1 \\ C_{l,Act,k} \\ C_{\mu,k} \\ \dot{C}_{\mu,k} \\ \alpha_k \\ C_{l,Act,k}C_{\mu,k} \\ C_{l,Act,k}\dot{C}_{\mu,k} \\ C_{l,Act,k}\alpha_k \\ C^2_{\mu,k} \\ C_{\mu,k}\dot{C_{\mu,k}} \\ C_{\mu,k}\alpha_k \\ \dot{C}^2_{\mu,k} \\ \dot{C}_{\mu,k}\alpha_k \\ \alpha^2_k \end{bmatrix} \tag{4}$$

Note: we remove the term $C^2_{l,Act,k}$ because the roll moment can take positive and negative values, and an even term will only create symmetric behavior which is not desired.

The SINDy problem to solve is:

$$C_{l,Act,k+1} = \Xi\Theta(C_{l,Act,k}, C_{\mu,k}, \dot{C}_{\mu,k}, \alpha_k) \tag{5}$$

We solve this regression problem using the STLS regression method described in Section III, and sweep the value of the parameter λ to explore a large set of combinations of these different nonlinear candidates. We ended with a model for $\alpha = 0°$ and $10°$ and another model for $\alpha = 20°$ using this algorithm. To identify the model at $\alpha = 0°$ and $10°$, we concatenated the time-series at these two angles of attack. The first half of the measurements are done at $0°$ and the rest at $10°$. The result of the identification is presented in the Fig. 7.

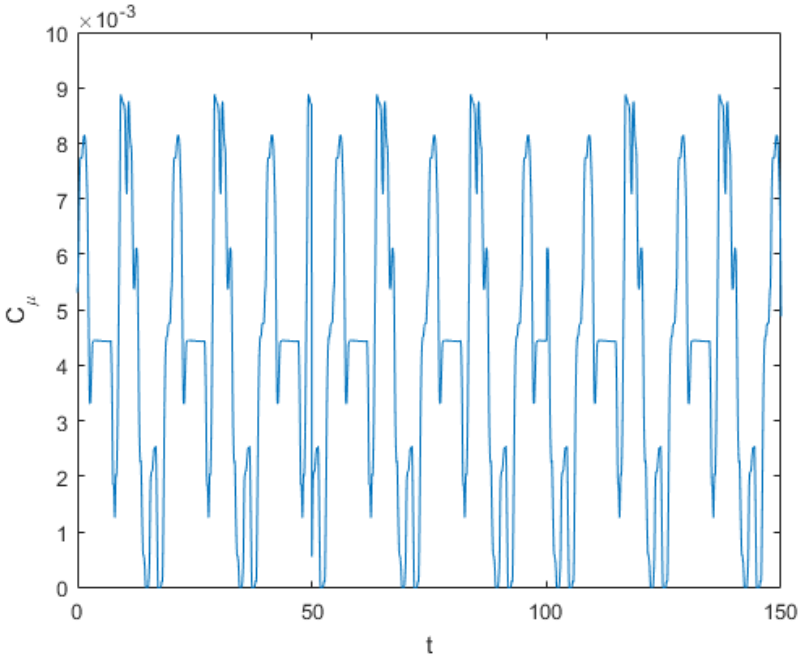

Figure 6: Random actuation with holds, Brunton, et al.[8]

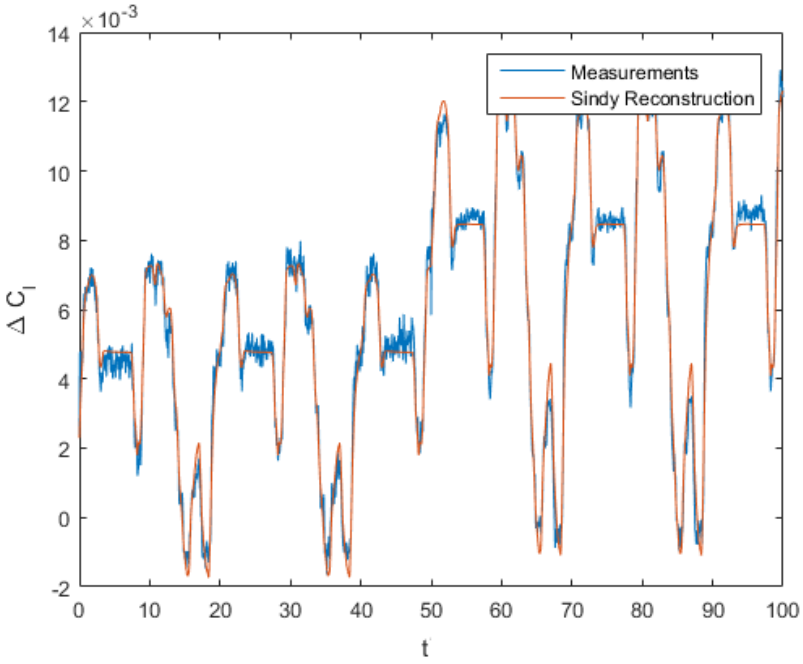

Figure 7: Measurement of roll moment with actuation(blue), SINDy prediction (orange) of the roll moment with a random actuation with holds versus time for $\alpha = 0°$ and $10°$.

The active terms in the model for $\alpha = 0°$ and $10°$ are:

$$\begin{bmatrix} 1 & C_{l,Act,k} & C_{\mu,k} & \dot{C_{\mu,k}} & C_{l,Act,k}C_{\mu,k} & C_{l,Act,k}\dot{C}_{\mu,k} & C_{l,Act,k}\alpha_k & C^2_{\mu,k} & C_{\mu,k}\dot{C}_{\mu,k} \end{bmatrix}^T \tag{6}$$

For $\alpha = 20°$, the active terms are:

$$\begin{bmatrix} C_{l,Act,k}C_{\mu,k} & C_{l,Act,k}\dot{C}_{\mu,k} & C_{l,Act,k}\alpha_k & C^2_{\mu,k} & C_{\mu,k}\dot{C}_{\mu,k} & C_{\mu,k}\alpha_k \end{bmatrix}^T \tag{7}$$

The Fig.7 shows the SINDy prediction of the roll moment with a random actuation with holds on the port side versus time for $\alpha = 0°$ and $10°$. We can conclude that our model is able to predict accurately most of the dynamic response of the roll moment. The measurements are still noisy at the holds (e.g $t = 5s$) and are not very repeatable, so our model is not able to capture these fluctuations.

IV. Results

The results presented in this section assess the validity of the principle of superposition in our system model. We analyze measurements in three cases; namely, with roll motion and no actuation, without roll motion and with actuation, and with roll motion and actuation. The optimal operator will be designed with cases where the roll moment response to disturbances is estimated from our disturbance model and the roll moment response to actuation computed from our plant model.

Datasets of the roll moment from measurements done at different angles of attack $\alpha = 0°, 10°$ and $20°$ were acquired. The first dataset is composed of measurements with random roll motion without actuation at these different angles of attack. The different measurements for each angle of attack are then concatenated together. The roll motion used is a random motion with holds similar to the input use for the actuation in Fig.6 with $\phi \in [-30°, 30°]$. The second dataset is composed of measurements with random actuation on the port side of the wing described in the Fig.6 without roll motion at the three different angles of attack and the different measurements for each angle of attack are then concatenate together. The third dataset is composed of measurements with the same random roll motion and random actuation on the port side of the wing at these different angles of attack and the different measurements for each angle of attack are then

concatenated together. The signal for the actuation is delayed by $8s$ from the signal for the open-loop roll angle in the last set of measurements to get independent roll motion and actuation.

In the remainder of this section, all the following plots and comments will be based on these three datasets at the angles of attack $\alpha = 0°, 10°,$ and $20°$. The first $50s$ of the following plots will be from measurements done at $\alpha = 0°$. The section of the plots from $50s$ to $100s$ will be from measurements done at $\alpha = 10°$. The last $50s$ of the time series from $100s$ to $150s$ will be from measurements done at $\alpha = 20°$.

Fig.8 compares the measurement of C_l with roll motion and actuation(blue) and the sum of C_l with roll motion and non actuation, and C_l without roll motion and actuation (orange) for $\alpha = 0°, 10°,$ and $20°$. If our system is linear, then we will get a perfect match between these two curves. However, there is a non-zero difference between these curves, which increases in amplitude with the angle of attack. Fig.9 shows the difference between the two previous curves for $\alpha = 0°, 10°$ and $20°$. We can quantify the deviation from the principle of superposition by computing the following adimensioned deviation defined as the ratio of the standard deviation of $\Delta C_l = C_{l,RollAFC} - C_{l,Roll} - C_{l,AFC}$ over the mean value of the roll moment with actuation and disturbances $C_{l,RollAFC}$ for the different angles of attack. Results are summarized in Tab.1 for the different angles of attack.

	$\alpha = 0°$	$\alpha = 10°$	$\alpha = 20°$
$\sigma(\Delta C_l)/\bar{C}_{l,RollAFC}$	11%	15%	30%

Table 1: $\sigma(\Delta C_l)/\bar{C}_{l,RollAFC}$ for the different angles of attack

For $\alpha = 0°$ ($t = 0s - 50s$), we obtain $\sigma(\Delta C_l)/\bar{C}_{l,RollAFC} = 11\%$. This adimensioned deviation from the linear theory is important. Nonetheless, we should be cautious with this result as the ratio noise to signal is high for low angles of attack. Therefore the real value of this adimensioned deviation will be less, such that we can still assume that the system behaves linearly and the error is mainly due to noise in the measurements. For $\alpha = 10°$ ($t = 50s - 100s$), the adimensioned deviation is 15%, but the ratio noise to signal is lower than for $\alpha = 0\%$. From this result, we see that nonlinear effects are becoming important and have to be considered in the design of the controller. The roll moment difference ΔC_l reach maximum of amplitudes when there are fast changes in the roll moment. For $\alpha = 20°$ ($t = 100s - 150s$), the adimensioned deviation reaches 30%, and nonlinear effects are very important.

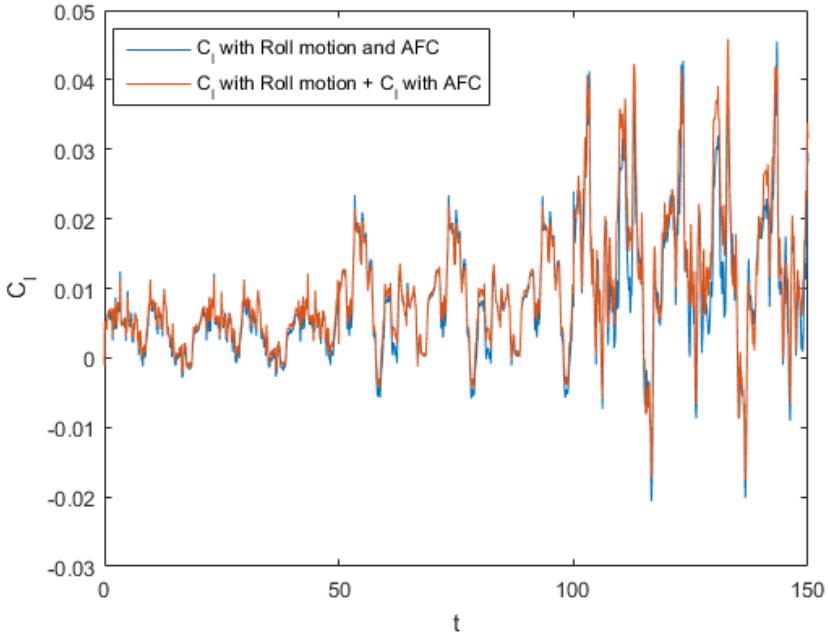

Figure 8: Measurement of C_l with roll motion and actuation (blue), sum of C_l with roll motion and non actuation, and C_l without roll motion and actuation (orange) for $\alpha = 0°(t = 0s - 50s), 10°(t = 50s - 100s)$, and $20°(t = 100s - 150s)$

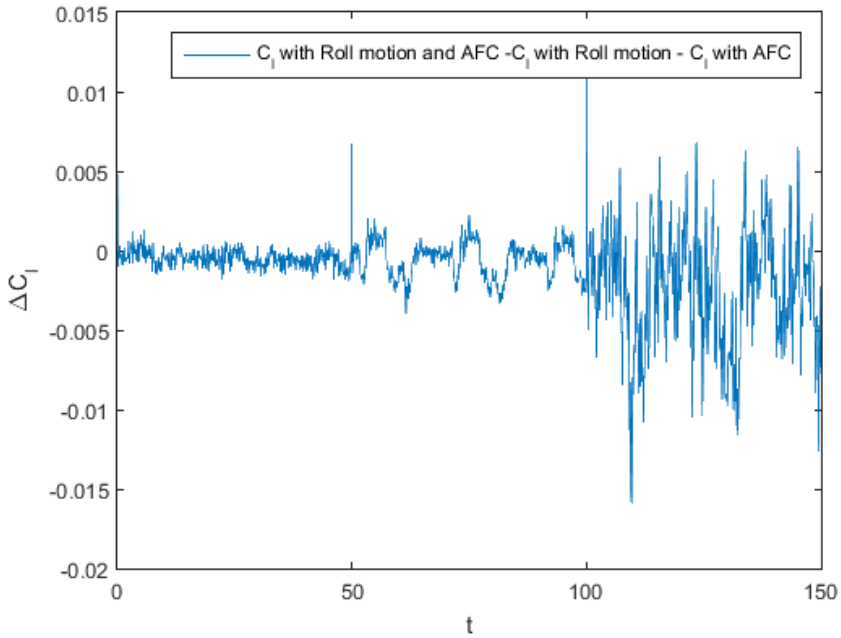

Figure 9: C_l with roll motion and actuation - C_l with roll motion and non actuation - C_l without roll motion and actuation (blue) for $\alpha = 0°(t = 0s - 50s), 10°(t = 50s - 100s)$ and $20°(t = 100s - 150s)$

V. Design of the optimal operator using the SINDy approach to account for coupling effects

In the previous section, we have shown that the flow field has measurable nonlinear effects, and the principle of superposition has some error. Based on this result we attempt to improve the final prediction of the roll moment by adding a nonlinear function $f(C_{l,Roll,k}, C_{l,AFC,k}, \alpha_k, C_{\mu,k})$ to account for coupled contributions of the disturbance and actuation responses.

We will use the SINDy algorithm to design the appropriate operator to get the overall response of the system, given its behavior to actuations and disturbances.

$$C_{l,RollAFC,k} = C_{l,Roll,k} + C_{l,AFC,k} + f(C_{l,Roll,k}, C_{l,AFC,k}, \alpha_k, C_{\mu,k}) \tag{8}$$

So the SINDy problem to solve is:

$$C_{l,RollAFC,k} = C_{l,Roll,k} + C_{l,AFC,k} + \Xi\Theta(C_{l,Roll,k}, C_{l,AFC,k}, \alpha_k, C_{\mu,k}) \tag{9}$$

We can rewrite it as:

$$C_{l,RollAFC,k} - C_{l,Roll,k} - C_{l,AFC,k} = \Xi\Theta(C_{l,Roll,k}, C_{l,AFC,k}, \alpha_k, C_{\mu,k}) \tag{10}$$

To apply the SINDy algorithm, we first need to identify the correct pool of candidates. Some combinations of variables are not valid. Indeed if we turn off the actuation, we want this operator to return only the prediction of disturbance model. By the same way, when there are no disturbances, we want that this operator return only the prediction of the plant model. Therefore, we should remove the following non-admissible terms:

- 1, because any constant will add an offset when there is only the contribution from actuations or disturbances
- $Cl^2_{Roll,k}$ and $Cl^2_{AFC,k}$, because the roll moment can be negative or positive.
- α_k, because this term will add a non-zero contribution for a non-zero angle of attack which is not desired.
- C_μ, because this term will add a non-zero contribution when there is actuation but no roll motion, which is not desired.

The pool of nonlinear candidates is:

$$\Theta(C_{l,Act,k}, C_{\mu,k}, \dot{C_{\mu,k}}, \alpha_k) = \begin{bmatrix} C^3_{l,d,k}\bar{\delta}(C_\mu) \\ C^3_{act,d,k}\bar{\delta}(\phi) \\ C_{l,d,k}C_{act,d,k} \\ C_{l,d,k}C_{\mu,k} \\ C_{l,d,k}\dot{C}_{\mu,k} \\ C_{l,d,k}C_{act,d,k}\alpha_k \\ C_{l,d,k}C^2_{act,d,k} \\ C^2_{l,d,k}C_{act,d,k} \\ C_{l,d,k}C_{\mu,k}\dot{C}_{\mu,k} \\ C_{l,d,k}C^2_{\mu,k} \\ C_{l,d,k}\dot{C}^2_{\mu,k} \\ C_{l,d,k}C^2_{act,d,k}\alpha_k \\ C^2_{l,d,k}C_{act,d,k}\alpha_k \\ C^2_{l,d,k}C^2_{act,d,k}\alpha_k \end{bmatrix} \tag{11}$$

where $\bar{\delta}(x) = 1 - \delta(x)$ is the anti-Dirac delta function which returns 0 if $x = 0$ or 1 for $x \neq 0$. Using this function, we can guarantee that the term $C^3_{l,d,k}\bar{\delta}(C_\mu)$ will be active only when there is actuation. Similarly, $C^3_{l,act,k}\bar{\delta}(\phi)$ will be active only when there are roll disturbances.

Three different datasets of roll moment from estimation, from models or measurements done at different angles of attack $\alpha = 0°, 10°$ and $20°$ were used. The first dataset is composed of estimation of the roll moment using the coupled disturbance model presented in §III with random roll motion without actuation at these different angles of attack. The different measurements for each angle of attack are then concatenated together. The roll motion used is a random motion with holds similar to the input use for the actuation in Fig.6 with $\phi \in [-30°, 30°]$. The second dataset is composed of estimates of the roll moment using the SINDy model for the actuation model presented in §III with random actuation on the port side of the wing described in the Fig.6 without roll motion at the three different angles of attack and the different measurements for each angle of attack are then concatenate together. The third dataset is composed of measurements with the same random roll motion and random actuation on the port side of the wing at these different angles of attack and the different measurements for each angle of attack are then concatenated together. The signal for the actuation is delayed by $8s$ from the signal for the roll angle in the last set of measurements to get independent roll motion and actuation.

We swept again for different values of λ to identify the best sparse solution to this problem, and ended with the following active terms with the appropriate coefficients:

$$\begin{bmatrix} -213.25C_{l,d,k}^3\bar{\delta}(C_\mu) \\ -462.14C_{act,d,k}^3\bar{\delta}(\phi) \\ 3.35C_{l,d,k}C_{act,d,k} \\ 1.17C_{l,d,k}C_{\mu,k} \\ 0.23C_{l,d,k}\dot{C}_{\mu,k} \\ 1528.44C_{l,d,k}C_{act,d,k}^2 \\ -2135.83C_{l,d,k}^2C_{act,d,k} \\ -1.54C_{l,d,k}C_{\mu,k}^2 \\ 0.35C_{l,d,k}\dot{C}_{\mu,k}^2 \\ -151.77C_{l,d,k}C_{act,d,k}^2\alpha_k \\ 111.84C_{l,d,k}^2C_{act,d,k}\alpha_k \\ 1393.90C_{l,d,k}^2C_{act,d,k}^2\alpha_k \end{bmatrix} \tag{12}$$

The interesting result is the presence of cross-terms between the disturbance contribution and the actuation contribution, such as, the terms $C_{l,Roll,k}C_{l,AFC,k}$ and $C_{l,Roll,k}^2C_{l,AFC,k}\alpha_k$ $C_{l,Roll,k}C_{l,AFC,k}^2\alpha_k$. The very large coefficient 1393.90 in front of $C_{l,d,k}^2C_{act,d,k}^2\alpha_k$ should be considered carefully, because the term $C_{l,d,k}^2C_{act,d,k}^2\alpha_k$ is order of magnitude of 10^{-6}. In the end, this term is a relatively small correction of the linear assumption compared to the others. The most important corrections are the terms $1.17C_{l,d,k}C_{\mu,k}$, $-1.54C_{l,d,k}C_{\mu,k}^2$, , $111.84C_{l,d,k}^2$, $-151.77C_{l,d,k}C_{act,d,k}^2\alpha_k$ and $111.84C_{l,d,k}^2C_{act,d,k}\alpha_k$.

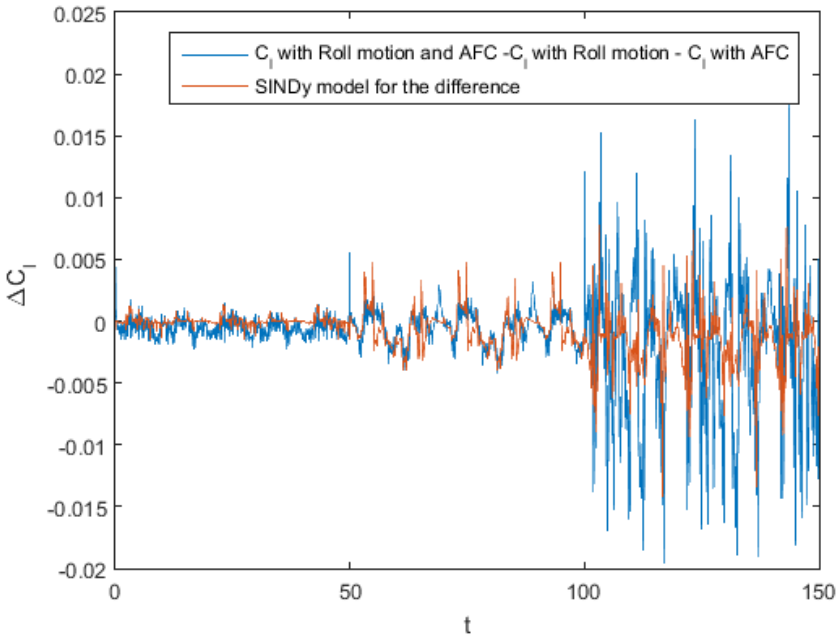

Figure 10: C_l with roll motion and actuation - C_l with roll motion and non actuation - C_l without roll motion and actuation(blue), SINDy model for the difference (orange).

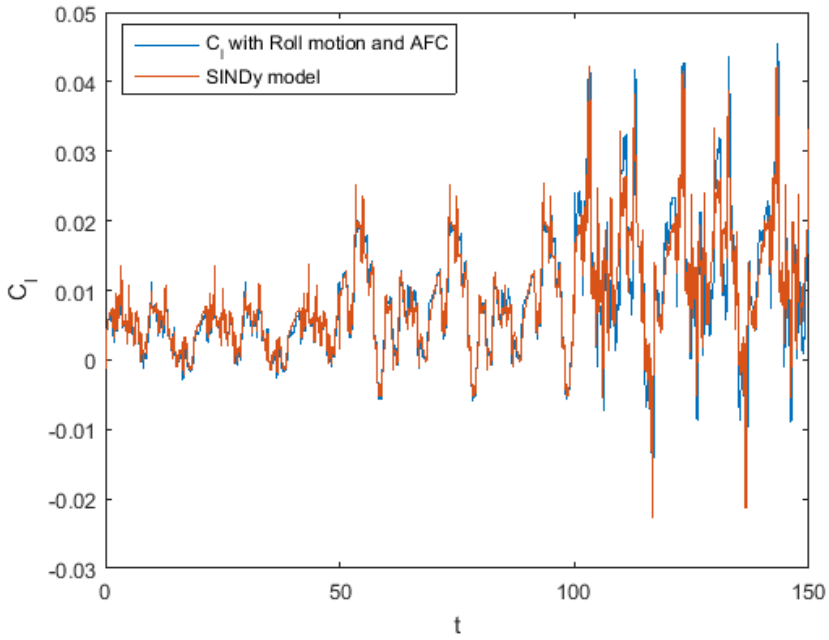

Figure 11: Measurement of C_l with roll motion and actuation(blue), prediction from SINDy for C_l with roll motion and actuation (orange)

Fig.10 shows the difference between C_l with roll motion and actuation, and C_l with roll motion and non actuation, and C_l without roll motion and actuation and the SINDy model for the difference. Again, if we have a purely linear system with the principle of superposition perfectly valid, the blue curve which is the difference between C_l with roll motion and actuation with C_l with roll motion and non actuation and C_l without roll motion and actuation and the SINDy model for the difference will be identically equal to 0. Nonetheless, there is a non-zero difference which means that the system behaves nonlinearly. Therefore, we try to model this difference using the SINDy algorithm which is the curve in orange in the Fig.11.

Fig.11 shows the reconstruction of the roll moment with combined roll motion and actuation using the identified SINDy model. Therefore, the main dynamics of the nonlinear term (curve blue) are captured by our SINDy model (curve orange). We compute the different errors $E_{lin,\alpha}$ and $E_{SINDy,\alpha}$. $E_{lin,\alpha}$ is the norm of the error between the roll moment $C_{l,RollAFC}$ we have from measurements with roll motion and actuation, and the roll moment we get if we simply add the contribution of the disturbance and actuation models to the roll moment for the angle of attack α. $E_{SINDy,\alpha}$ is the norm of the error between the real $C_{l,RollAFC}$ we have from measurements with roll motion and actuation, and the roll moment we get with the correction term designed with the SINDy algorithm added to the estimation of the roll moment response to actuation and disturbance from models for the angle of attack α. In other words, we have the following formulas for $E_{lin,\alpha}$ and $E_{SINDy,\alpha}$:

$$E_{lin,\alpha} = ||C_{l,RollAFC,k} - C_{l,Roll}^{model} - C_{l,AFC}^{model}||_2 \tag{13}$$

$$E_{SINDy,\alpha} = ||C_{l,RollAFC} - C_{l,Roll}^{model} - C_{l,AFC}^{model} - \Xi\Theta(C_{l,Roll}^{model}, C_{l,AFC}^{model}, \alpha, C_\mu)||_2 \tag{14}$$

	$\alpha = 0°$	$\alpha = 10°$	$\alpha = 20°$
$E_{SINDy,\alpha}/E_{lin,\alpha}$	99%	90%	85%

Table 2: Error improvement with the SINDy correction

Tab.2 shows the improvement of the error for the different angles of attack. For $\alpha = 0°$, we get $\frac{E_{SINDy,\alpha=0°}}{E_{lin,\alpha=0°}} = 0.99$, i.e. a reduction of the error of 1%. Indeed, as the principle of superposition holds for 0°, it seems reasonable that there is no significant improvement of the error. For $\alpha = 20°$, we get $\frac{E_{SINDy,\alpha=20°}}{E_{lin,\alpha=20°}} = 0.85$, so we reduce the error by 15% if we add this optimal operator designed with the SINDy algorithm.

We also computed for the different angles of attack, the correlation coefficient between the roll moment coefficient with actuation and roll motion with the prediction where we just sum both contributions. Results are presented in Tab.3. For $\alpha = 0°$ and 10°, there is only a slight increase in the correlation coefficient but for $\alpha = 20°$, we are increasing the correlation coefficient from 0.8423 with linear assumption to 0.8699 with the SINDy correction. Through our nonlinear correction, we simultaneously correct and model two phenomenona: the nonlinear behavior of the flowfield itself and the imperfection of the low-dimensional plant and disturbance models.

	$\alpha = 0°$	$\alpha = 10°$	$\alpha = 20°$
$Corrcoeff_{LinearAssumption}$	0.9752	0.9803	0.8423
$Corrcoeff_{OptimalOperator}$	0.9768	0.9863	0.8699

Table 3: Correlation coefficient with the linear assumption and SINDy correction

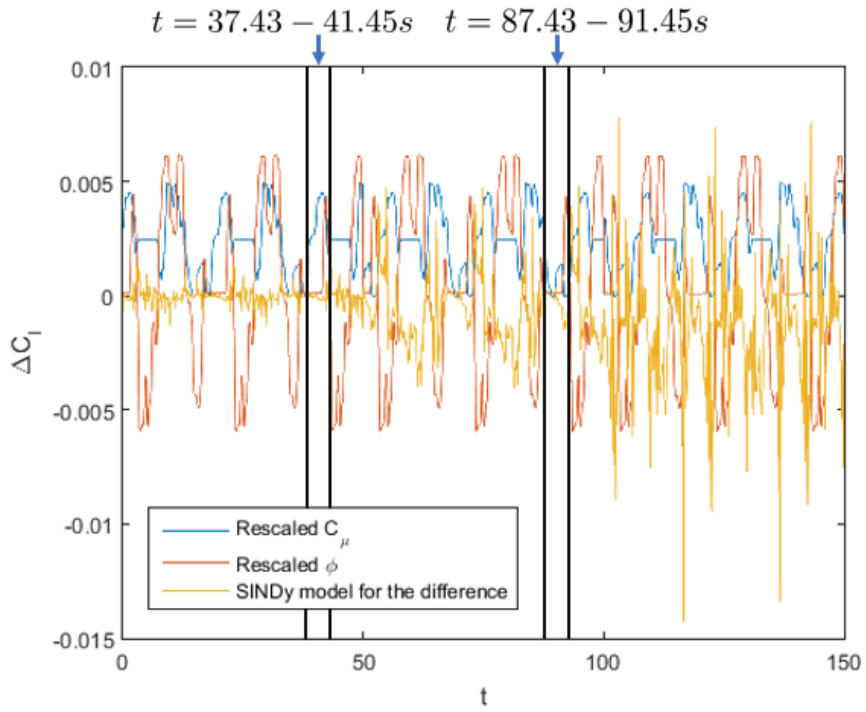

Figure 12: Scaled C_μ(blue), Scaled ϕ(orange), SINDy model for the difference(yellow)

As highlighted in the previous section, the nonlinear behavior of the flow field increases with the angle of attack. Let us determine which other parameters of the flow field affect the nonlinear correction. Figure 12 shows the rescaled C_μ coefficient(blue), the rescaled roll angle ϕ(orange) and the nonlinear correction identified for the different angles of attack(yellow). Both C_μ and ϕ are rescaled by arbitrary constants to get the same order of magnitude as the nonlinear correction, and plot the three curves on the same figure. For $\alpha = 0°$ and $10°$ (i.e. $t = 0 - 100s$), the amplitude of the nonlinear term is determined by the variation of the roll angle ϕ and not by the momentum coefficient. Indeed, when $\phi = 0°$ the nonlinear correction is close to 0 whatever the value of C_μ, e.g. $t = 37.43 - 41.45s$ for $\alpha = 0°$ and $t = 87.43 - 91.45s$ for $\alpha = 10°$. Nonetheless, for $\alpha = 20°$, the correction term does not exhibit such simple behavior and depends non-linearly of both ϕ and C_μ.

Finally, we assess the robustness of our correction by adding noise to our data. The noise is chosen to be Gaussian with a mean value $\mu = 0$ and standard deviation $\sigma = 0.001$.

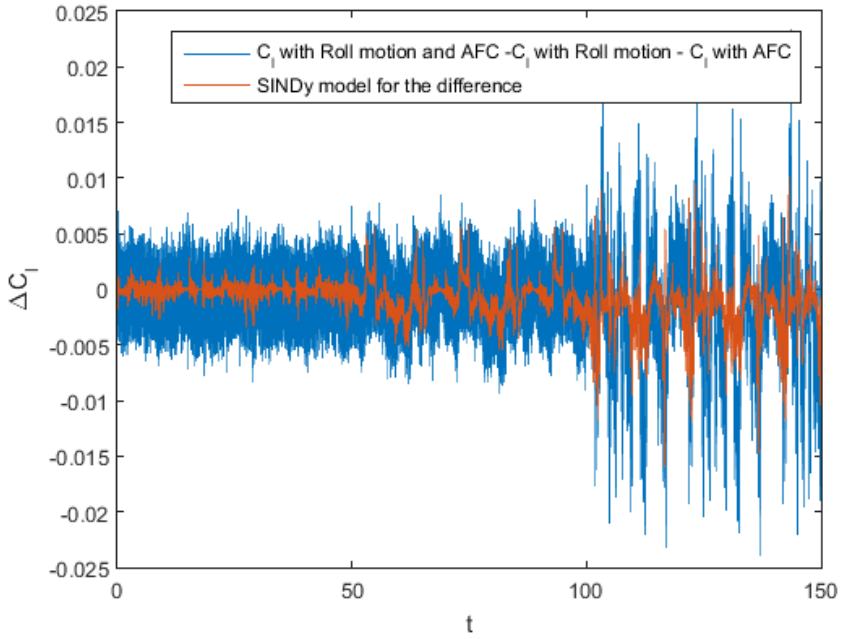

Figure 13: C_l with roll motion and actuation - C_l with roll motion and non actuation - C_l without roll motion and actuation(blue), SINDy model for the difference (orange)

Figure 13 shows the difference between C_l with roll motion and actuation, and C_l with roll motion and non actuation, and C_l without roll motion and actuation and the SINDy model for the difference with added Gaussian noise$\sim \mathcal{N}(0, 0.001)$ to the data. Even with highly noisy data, the SINDy correction is very similar to the one obtained without noise in Figure 10. We also compute the correlation coefficient with the linear assumption and the nonlinear correction. We get $Corrcoeff_{LinearAssumption} = 0.8820$. We did the same procedure with the optimal operator designed with SINDy, so we have $Corrcoeff_{OptimalOperator} = 0.8924$. This test demonstrates that our correction is robust to noise. Moreover, for all the different standard deviations σ of noise tested, the nonlinear combination always overruled the linear combination of the plant and disturbance response.

VI. Conclusions

A robust model for the prediction of the roll moment for periodic and pseudo-random motions is constructed by coupling a linear model based on the pressure and an extended Goman-Khrabrov model. The coupled approach is efficient, because it allows us to take advantage of both prediction models. The linear pressure-based model is very good at predicting the main trend of the roll moment, and the extended Goman-Khrabrov model is efficient at reproducing the fluctuations of the roll moment.

We also obtained a robust plant model G_p for the actuation using the SINDy algorithm.

The validity of the principle of superposition for flow control is investigated and we conclude that the principle of superposition gives an error up to 10% in the prediction of the roll moment based on measurements.

We showed that we can reduce this error by designing an optimal operator to couple the contributions of the actuations and roll disturbances to the roll moment. This coupling will allow better performance of the closed-loop controller, as we will get a more accurate estimation of the roll moment. A reduction of 15% of the error with the optimal operator designed with the SINDy algorithm was achieved for $\alpha = 20°$.

SINDy method is particularly suitable for implementation in real-time controllers and critical systems(e.g. flight controllers). First, the runtime of this model is very low and therefore can be handled by an embedded system. Second, the SINDy method allows a refined design of the correction, we can simply choose the relevant candidates in the dynamic of the system we want to keep or remove. Finally, the SINDy decomposition

intrinsically promotes robustness through the sparse regression Kaiser, et al.[9]

Acknowledgments

We are grateful for the support from the Office of Naval Research with Grant N00014-16-1-2622 and program managers Ken Iwanski and Brian Holm-Hansen.

References

[1]Brunton, S. L., Proctor, J. L., and Kutz, J. N., "Discovering governing equations from data by sparse identification of nonlinear dynamical systems," *Proceedings of the National Academy of Sciences*, Vol. 113, No. 15, 2016, pp. 3932–3937.

[2]Williams, D. R., An, X., Iliev, S., King, R., and Reißner, F., "Dynamic hysteresis control of lift on a pitching wing," *Experiments in Fluids*, Vol. 56, No. 5, 2015, pp. 112.

[3]Kerstens, W., Pfeiffer, J., Williams, D., King, R., and Colonius, T., "Closed-loop control of lift for longitudinal gust suppression at low Reynolds numbers," *AIAA journal*, Vol. 49, No. 8, 2011, pp. 1721–1728.

[4]Budišić, M., Mohr, R., and Mezić, I., "Applied koopmanism a," *Chaos: An Interdisciplinary Journal of Nonlinear Science*, Vol. 22, No. 4, 2012, pp. 047510.

[5]Le Provost, M., He, X., and Williams, D. R., "Real-time Roll and Pitching Moment Identification with Distributed Surface Pressure Sensors on a UCAS Wing," *57th AIAA Aerospace Sciences Meeting (AIAA SciTech)*, 2018.

[6]Goman, M. and Khrabrov, A., "State-space representation of aerodynamic characteristics of an aircraft at high angles of attack," *Journal of Aircraft*, Vol. 31, No. 5, 1994, pp. 1109–1115.

[7]Brunton, B. W., Johnson, L. A., Ojemann, J. G., and Kutz, J. N., "Extracting spatial–temporal coherent patterns in large-scale neural recordings using dynamic mode decomposition," *Journal of neuroscience methods*, Vol. 258, 2016, pp. 1–15.

[8]Brunton, S. L. and Rowley, C., "Unsteady aerodynamic models for agile flight at low Reynolds numbers," *48th AIAA Aerospace Sciences Meeting and Exhibit*, 2010.

[9]Kaiser, E., Kutz, J. N., and Brunton, S. L., "Sparse identification of nonlinear dynamics for model predictive control in the low-data limit," *arXiv preprint arXiv:1711.05501*, 2017.